JMEPEG
https://doi.org/10.1007/s11665-024-09513-4

1059-9495/$19.00

ORIGINAL RESEARCH ARTICLE

Manufacturing of High Purity Cr_2AlC MAX Phase Material and Its Characterization

Vyom Desai, Aroh Shrivastava, Arunsinh B. Zala, Tejas Parekh, Surojit Gupta, and N.I. Jamnapara

Submitted: 27 September 2023 / Accepted: 12 March 2024

Present study discusses about a technique for producing high-purity Cr_2AlC MAX phase materials and gaining insight into their thermal behavior for high-temperature applications. The research conducted involved synthesizing a pure layered ternary carbide Cr_2AlC MAX phase material by mixing powders of Chromium, Aluminum, and Carbon and then subjecting them to two-step pressureless sintering process in argon atmosphere. First step involves the annealing of ball-milled mixture at 750 °C for 2 h followed by the second step in which the annealed mixture is subjected to heat-treatment at 1350 °C for 2 h. Analysis using XRD and Raman techniques revealed that the synthesized product consists of Cr_2AlC phase, without any impurities. SEM studies confirmed that the Cr_2AlC had a layered topography, while EPMA analysis indicated that the atomic percentage of Cr, Al, and C was consistent with the XRD phase analysis. XPS investigations confirmed the presence of Cr-C bonds representing $M_{n+1}X_n$ of the MAX phase material. TG-DSC results showed an approximately 2% increase in weight. The Cr_2AlC phase exhibited an endothermic pattern below 725 °C, an exothermic pattern above it, and did not decompose up to 1400 °C in vacuum environment. High-temperature XRD analysis at various temperatures also confirmed no formation of Al_2O_3 or CrO impurity compounds.

Keywords Cr_2AlC, MAX phases, powder metallurgy, pressureless sintering

1. Introduction

MAX phase materials are a unique category of materials that exhibit a distinctive combination of metallic and ceramic characteristics. They consist of ternary layered nitrides and carbides with a general chemical formula of $M_{n+1}AX_n$, where M denotes an early transition metal, A represents a predominantly IIIA- or IVA-group element, and X can be either carbon or nitrogen (Ref 1). These MAX phases possess a hexagonal crystal structure and belong to the P63/mmc space group (Ref 2). Noteworthy properties of MAX phase materials include high thermal conductivity, exceptional strength, excellent machinability, strong resistance to corrosion, high temperature oxidation resistance, low density, and low thermal expansion coefficient (Ref 3-7). Currently, a combination of theoretical and experimental studies has documented approximately 150 distinct compositions of MAX phases (Ref 8).

Cr_2AlC belongs to the MAX phase family of materials, which was initially discovered by Jeitschko et al. (Ref 9) in 1963 and later confirmed by Schuster et al., in 1980 (Ref 10). It possess several notable properties, including high elastic modulus (Ref 7), excellent corrosion resistance against Na_2SO_4 at approximately 1000 °C (Ref 7), excellent oxidation resistance up to 1300 °C (Ref 7), excellent radiation resistance (Ref 11), good mechanical properties at room temperature (Ref 12). Additionally, Tian et al, reported that Cr_2AlC exhibits good electrical conductivity ranging from 1.4 to 2.3 $\times$ 10^{-6} Ω^{-1} m^{-1} and thermal conductivity ranging from 17.5 to 22.5 W/m K (Ref 13). It has been observed that the corrosion and oxidation resistance of Cr_2AlC surpasses that of Ti_3AlC_2 and Ti_3SiC_2 (Ref 7, 14). These properties render Cr_2AlC suitable for various applications involving graphite-metal composites, such as electrical plates, pantographs, bipolar plates in fuel cells, and photocatalysis, among others (Ref 8, 15). Furthermore, its high temperature oxidation resistance makes it suitable for use in the nuclear industry, structural applications, and gas burner nozzles (Ref 16).

Various methods have been employed for the synthesis of Cr_2AlC including Hot pressing (HP) (Ref 17), spark plasma sintering (SPS) (Ref 18), pressureless sintering, molten salt method (Ref 19) and hot isostatic pressing (HIP) (Ref 20). Manoun et al., achieved successful synthesis of Cr_2AlC by mixing of Cr, Al, and C, utilizing HIP method at a temperature of 1200 °C and an approximate pressure of 100 MPa (Ref 20). Conversely, Yukhvid et al. prepared Cr_2AlC using precursors such as Cr_2O_3, CrO_3, Al, and C through the self-propagating high-temperature synthesis (SHS) method under an argon atmosphere at a pressure of 5 MPa (Ref 21). Additionally, Zhou et al. investigated the reaction kinetics and mechanical properties of Cr_2AlC synthesized via the hot pressing technique at 1300 °C and at 30 MPa pressure (Ref 22). Cr_2AlC were synthesized by Li et al, at relatively lower temperature at 1100 °C and 30 MPa using Hot Pressing (Ref 17). However, it

Vyom Desai, Aroh Shrivastava, and **N.I. Jamnapara**, Institute For Plasma Research, Bhat, Gandhinagar 382428, India; and Homi Bhabha National Institute, Training School Complex, Anushaktinagar, Mumbai 400094, India; **Arunsinh B. Zala** and **Tejas Parekh**, Institute For Plasma Research, Bhat, Gandhinagar 382428 India; and **Surojit Gupta**, Department of Mechanical Engineering, University of North Dakota, Grand Forks. Contact e-mail: vyomdesai94@gmail.com.

Published online: 13 May 2024

is important to note that these processes typically require elevated temperatures exceeding 1000 °C, high pressures of up to 100 MPa, and complex equipment, which restricts their widespread applicability (Ref 23).

The production of high-quality Cr_2AlC powder presents a significant challenge due to various factors discussed in previous studies, including the low melting point of Al above 660 °C, the intense exothermal interaction between Cr and C, and the degradation of Cr_2AlC beyond 1400 °C (Ref 17, 24). Despite considerable advancements in this area, there remains a gap in achieving the synthesis of Cr_2AlC with high purity, as impurities such as Cr_7C3 and Cr_2Al phases are often observed alongside Cr_2AlC (Ref 25, 26). While techniques like hot pressing, hot isostatic pressing, and spark plasma sintering have been explored, their cost-effectiveness makes them impractical for continuous or bulk manufacturing. However, the pressureless sintering method provides an affordable and excellent option for mass production, enabling the creation of samples with complex and large shapes. Julian et al, reported less degradation of Cr_2AlC when employing pressureless sintering (Ref 27). Panigraphi et al. reported the synthesis of Cr_2AlC using pressureless sintering by initially forming partially sintered CrC_x powder and subsequently mixing it with Al (Ref 28). The production of CrC_x powder occurred at 1550 °C, followed by a mixing with Al, and subsequent furnace treatment to create Cr_2AlC at 1100 °C. This sequential procedure increases both the cost and time required for Cr_2AlC synthesis. A review of the literature revealed the necessity of achieving pure Cr_2AlC using pressureless sintering. The key challenges involve selecting the appropriate initial materials, potential formation of intermediate compounds during synthesis, Al oxidation during the reaction, the two-step sequential process, and the presence of impurities in the final Cr_2AlC product. Choi et al. and Tian et al. emphasized the importance of forming Cr_2Al in the synthesis of Cr_2AlC (Ref 24, 25). This paper introduces a novel two-step reaction strategy to achieve the synthesis of ultra-pure Cr_2AlC through pressureless sintering under an inert atmosphere. The method involves the initial formation of intermetallic Cr-Al compounds at 750 °C, followed by the subsequent reaction of these intermetallics with graphite to produce $C_{r2}AlC$ at 1350 °C.

MAX phases demonstrate exceptional suitability for high-temperature applications, emphasizing the significance of their oxidation and heat resistance properties. The stability of these materials under elevated temperatures stands as a pivotal subject for investigation. The remarkable oxidation resistance of Cr_2AlC has also been widely recognized. However, MAX phases, including Cr_2AlC, have a tendency to decompose at extremely high temperatures. For instance, Ti_3SiC_2 becomes unstable at temperatures exceeding 1400 °C in a vacuum or argon atmosphere (Ref 29-31), while Ti_3AlC_2 decomposes above 1400 °C in a vacuum environment (Ref 32, 33). In contrast, according to Xiao et al., Cr_2AlC demonstrates thermal stability in an argon atmosphere remaining stable up to 1500 °C (Ref 16). Lee at al. investigated the oxidation of Cr_2AlC in air upto 1200 °C (Ref 34), but information regarding the of thermal stability of Cr_2AlC in vacuum environment are scarce.

This study aims to establish a cost-effective synthesis method for obtaining pure Cr_2AlC without impurities. Additionally, it seeks to assess the thermal stability of Cr_2AlC in a vacuum environment by employing Differential Scanning Calorimetry and High Temperature x-ray Diffraction techniques.

2. Experimental Details

2.1 Synthesis of Cr_2AlC

The starting materials used to synthesize Cr_2AlC were powders of Chromium (≥ 99% trace metal basis, − 325 mesh, Sigma-Aldrich, St. Louis, MO), Al (99.5% trace metal basis, − 325 mesh, Alfa Aesar, Haverhill, MA), and graphite (Graphite powder crystalline, 99%, − 325 mesh, Alfa Aesar, Haverhill, MA). These precursors, viz. Cr, Al, and C were uniformly mixed using dry ball milling (8000 M mixer Mill; SPEX SamplePrep) in a molar ratio of 2:1.1:1, respectively. Similar molar ratios were already used for successful synthesis of Cr_2AlC by Hall et al. (Ref 35). Subsequently, the ball-milled powder was cold-pressed in to small pellets. These pellets are transferred into a tube furnace in which a continuously flowing Ar environment is maintained. These pellets are exposed to a thermal process cycle as shown in Fig. 1. The temperature inside the furnace was increased at a rate of 10 °C/min up to 750 °C, and the pellets were annealed for 2 h at this temperature. Then in the second step, the rate of heating was set at 5 °C/min till the heat treatment temperature i.e., 1350 °C is reached. At this temperature the heat treatment was carried out for 2 h. Then, the furnace was switched off and the pellets were cooled to room temperature through furnace cooling. A positive pressure of 1.1 bar is always maintained in the tube furnace in order to prevent the oxidation of Aluminum.

2.2 Characterization Techniques

The synthesized Cr_2AlC powders were characterized using various techniques including x-ray Diffraction (XRD), scanning electron microscopy (SEM), Electron Probe Micro analyzer (EPMA), Raman spectroscopy, and XPS. Cr_2AlC exhibits excellent oxidation resistance, and to understand its thermal stability at high temperatures in sub-atmospheric pressure, an assessment study was conducted using Differential Scanning Calorimetry and High-temperature XRD.

To identify the phases that are present in the powder, Cr_2AlC was subjected to XRD analysis using an XRD equipment (model: Bruker D8 discover, Supplier: Bruker GmbH, Germany) with Cu Kα radiation (λ = 1.5406 Å) in the 2θ range of 20-90° with a step size of 0.02° Bragg-Brentano mode. The crystallite size was computed using the Scherrer formula and the instrumental broadening was minimized by comparing the observed sample peak width (FWHM) to that of a typical reference sample. To investigate the thermal stability of Cr_2AlC, High temperature XRD was done using the Anton Par heating attachment in the same equipment. The High Temperature XRD was carried out in vacuum with a working pressure of 5×10^{-2} mbar to study the stability of Cr_2AlC and investigate whether that reversible phase transition occurred at high temperature. The base pressure of the HT-XRD system was 1×10^{-6} mbar. The step size for HT-XRD was 0.050, scan speed of 1 s/step and the ramp rate of 10 °C/min. The tube voltage was kept at 40 kV and tube current at 30 mA. The calibration of the high-temperature x-ray diffraction (HT-XRD) system involved the use of MgO as a standard reference material. This meticulous calibration process aimed to establish accurate relationships between the observed diffraction patterns and known characteristics of MgO, providing a reliable foundation for temperature-dependent XRD analyses. The Z axis calibration was also carried using MgO as standard

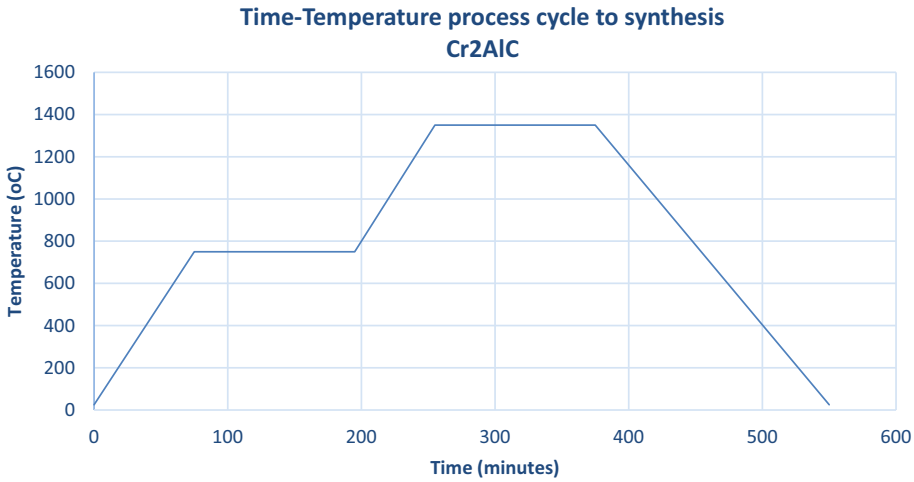

Fig. 1 Process cycle to synthesis Cr_2AlC

material at every temperature cycle. Consideration of the thermal response of the applied thermocouple is also important for the evaluation of the calibration results. The S-type Pt/Pt90-Rh10 thermocouple used in this study responds linear in the temperature range from approx. 350 up to 1200 °C.

Raman spectroscopy was performed to examine the vibrational, rotational and sample's structural characteristics with a confocal microscope (Model: Qontor by Renishaw). The spectrometer has a wavelength of 532 nm (He-Ne laser) and diffraction grating of 1200 grooves/mm.

The morphology of Cr_2AlC was studied using High resolution scanning electron microscopy (HRSEM; Model: Carl Zeiss, Supplier: VP Merlin, Germany) and its elemental composition was found out using electron probe micro analyzer (EPMA).

Cr_2AlC was studied using x-ray photoelectron spectroscopy (Model: Thermo-Scientific NEXSA) to determine its chemical states and bond energies. An excitation source employed was Al kα radiation with an energy of 1486.6 eV. The sample surface was sputter cleaned using an Ar ion beam at 3 keV for 5 min. The C1s peak, which corresponds to a binding energy of 284.6 eV, was used to calibrate the binding energy scale.

To determine the temperature-dependent phase changes, TG-DSC (Thermogravimetric and differential scanning calorimetry) study was carried out by a simultaneous thermal analyser (Model: Linseis GmbH, STA PT 1600). In the fused alumina crucibles, experiments on Cr_2AlC powder samples were carried out up to 1400 °C in vacuum at a pressure of 5×10^{-2} mbar. In the fused alumina crucibles, experiments on Cr_2AlC powder samples were carried out up to 1400 °C. The system's drift was assessed, and the results of the experiment were subtracted. The heating rate for the dynamic run was set to 10 °C per minute. The sample temperature was monitored using a type S thermocouple.

3. Results and Discussion

3.1 Reaction Mechanism

Figure 1 illustrates the process cycle employed in the synthesis of Cr_2AlC. As it is clear from this figure, the present pressureless sintering process consists of two main steps to facilitate the Cr-Al formation. (i) In the first step, the mixture of chromium, aluminum, and carbon is heated up to 750 °C and then annealed at this temperature for 2 h. This annealing temperature was chosen to be just above melting point of Aluminum, because of the following reason. At this temperature, Al will be in the molten state and the reaction rate between liquid Al and solid Cr would be much higher than that of between solid Al and solid Cr. As this annealing temperature is kept constant for sufficient time (2 h), the liquid aluminum selectively reacts with some chromium powders, either bonding with individual chromium atoms or forming chromium aluminides such as Cr_2Al and Cr_5Al_8. The carbon remains unreacted at this annealing temperatures. During the second step i.e., heat treatment at a high temperature of 1350 °C, the chromium-aluminum system undergoes complete reaction with carbon, resulting in the formation of Cr_2AlC. The synthesized product is furnace cooled to room temperature. The excess Al used in the process (1.1 moles instead of 1 mole), was required in order to compensate for any possible losses of Al that could arise during step 1 of the synthesis. The synthesized and cooled sample was then ground into very fine size with the help of agate mortar-pestle and sieved (325 mesh size), for further characterization.

3.2 X-ray Diffraction

The XRD spectra of Cr_2AlC synthesized at 1350 °C are shown in Fig. 2. The spectra revealed (103), (006), and (109) reflections that belong to the Cr_2AlC phase, as per ICDD file number 00-058-0267. A high-resolution scan was performed between 2θ values of 40° and 45°, in order to distinguish the very close peaks at 42.0716° and 42.1784° and both of these represent Cr_2AlC. The high-resolution XRD scan is shown in Fig. 3. Absence of peaks representing pure elements like Cr, Al, etc. or impurity compounds such as Cr_7C_3 Cr_2Al and Al_2O_3, in the XRD results, indicates about the synthesis of pure Cr_2AlC. Rietveld refinement were performed on the synthesized Cr_2AlC using Full PROF suite (Ref 36) and the lattice parameters of this layered Cr_2AlC were calculated, and the values for a, b, and c were found to be 2.862, 2.862, and 12.838 Å, respectively, which aligns with the values in the ICDD database file.

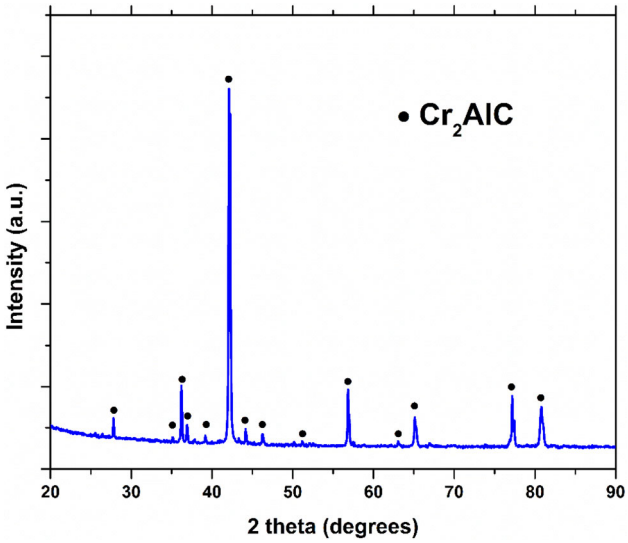

Fig. 2 X-ray diffraction pattern of synthesized Cr_2AlC powder

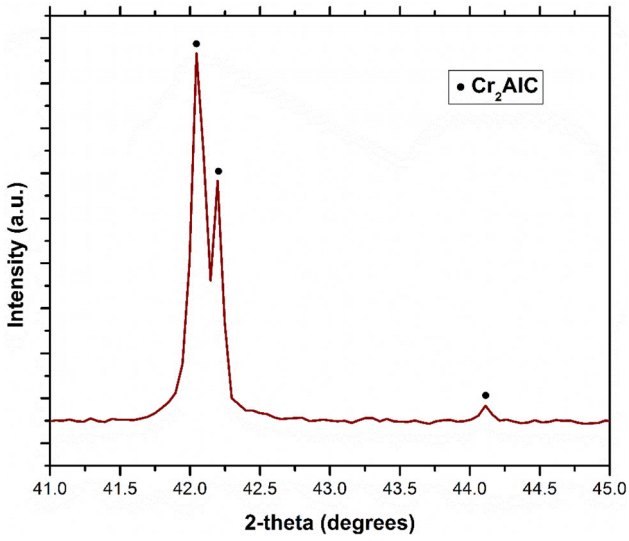

Fig. 3 High-resolution XRD pattern of synthesized Cr_2AlC

The crystallite size was calculated using Scherer's formula, and it was found to be around 102 nm.

3.3 Raman Spectroscopy

To confirm the single-phase synthesis of Cr_2AlC at 1350 °C as identified by XRD, Raman spectroscopy was employed to analyze its vibration bands. As shown in Fig. 4, all of the peaks observed in the Raman spectra of Cr_2AlC correspond to its vibrational bands. The MAX phases are classified under the $D4_{6h}$ space group and Raman signals are given in Table 1. The four Raman active optical modes belong to the 211 structures, three of which are Raman active i.e., 153.43, 245.53, 249.12 cm^{-1} and the one that is 335.74 cm^{-1} is both Raman and infrared active. (Ref 37-39). The wave numbers of the Raman spectra are given in Table 1, and they are in alignment with the theoretical data.

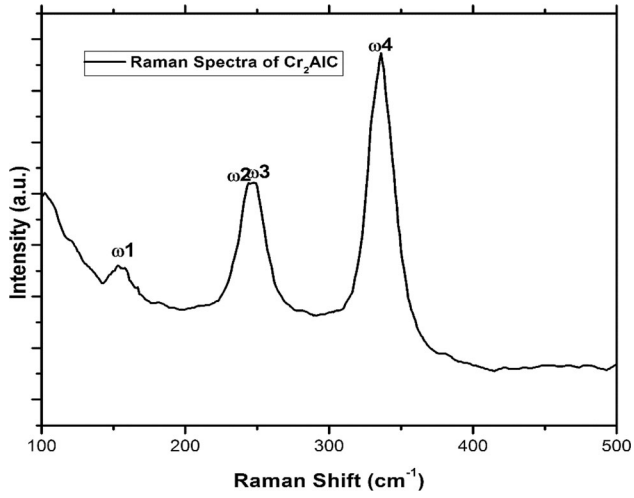

Fig. 4 Raman Spectra of the synthesized Cr_2AlC powder

Table 1 Wavenumbers (ω, in cm^{-1}), of the Raman modes of Cr_2AlC

	ω1 [E2g]	ω2 [E2g]	ω3 [E2g]	ω4 [E2g]
Cr_2AlC	153.43	243.53	249.12	335.74

3.4 SEM and EPMA

SEM was used for studying the morphology of the synthesized Cr_2AlC. The powder sample for SEM analysis was collected and sieved (325 mesh) to ensure uniformity, then mounted on a conductive substrate using carbon tape, followed by careful handling to prevent contamination. A conductive coating was not deemed necessary as Cr_2AlC is conductive in nature. SEM micrographs captured at various magnifications are shown in Fig. 5. It is clear from the SEM images that the synthesized Cr_2AlC is having a layered structure, and the average particle size is approximately 45 microns. During SEM studies, random EDS analysis of Cr_2AlC was performed and the results indicate that the average atomic percent of Cr is approximately 52.99%, whereas Carbon is approx. 24.19% and Al approx. 22.81%. EPMA studies were also performed for determining the elemental composition of Cr_2AlC. Point scans were conducted at five different locations and the results of the same are given in Table 2. The same results are shown in graphical form in Fig. 6. It is clear from these results that the elemental composition is in line with the stoichiometry of Cr_2AlC. These results are complimenting the XRD results.

3.5 X-ray Photoelectron Spectroscopy

Cr_2AlC, confirmed by x-ray diffraction (XRD) and Raman spectroscopy, was analyzed further using x-ray photoelectron spectroscopy (XPS) to gain insight into the bonding characteristics of this MAX phase material. The XPS core level binding energy spectra of Cr_2AlC were fitted using XPSPEAK 4.1 software. Figure 7 shows the fitted core level energy spectra for Cr2p, Al2p, C1s, and O1s of Cr_2AlC. As it can be seen from the results, the XPS analysis revealed the presence of oxygen. The reason for the presence of Oxygen is likely due to prolonged exposure of the synthesized powder to air, could

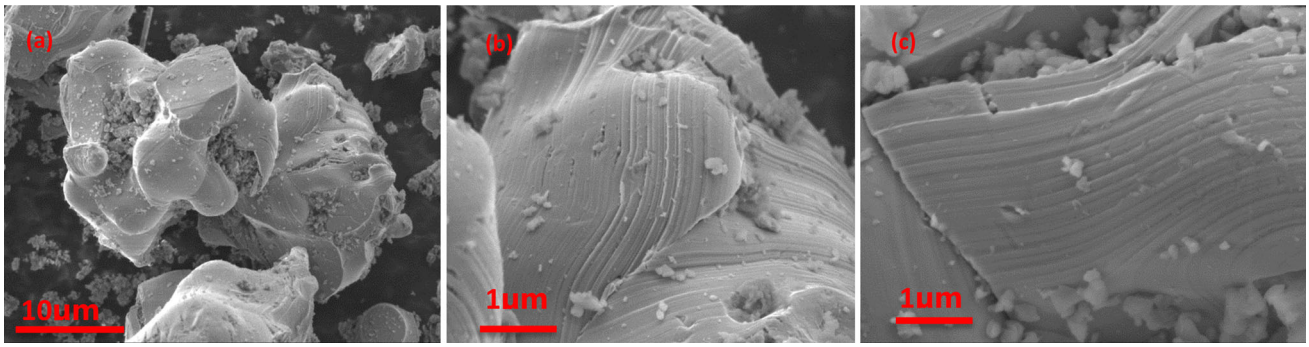

Fig. 5 SEM images of the synthesized Cr_2AlC at different magnifications (a) 2000X (b) 8500X (c) 20000X

Table 2 Atomic percentages of Cr, Al and C in MAX phase Cr_2AlC powder

Spectrum	Cr	Al	C
P1	58.88	21.47	19.65
P2	52.19	22.66	25.15
P3	51.99	25.17	22.89
P4	58.02	12.94	29.04
P5	46.8	25.94	27.26

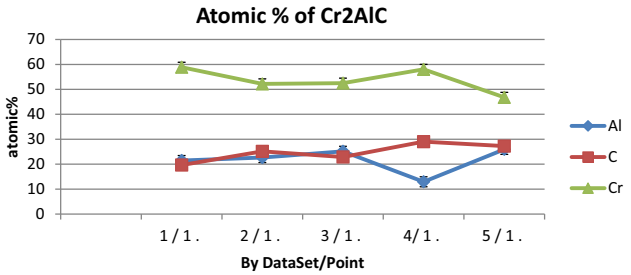

Fig. 6 Atomic percentage of Cr, Al and C in MAX phase Cr_2AlC powder

have lead to the formation of Cr and Al oxides. However, the absence of any oxide peaks in XRD, and Oxygen in EPMA results indicates that these oxides must have formed as thin layers on the surface only. Abedlkader reported that selective oxidation of Cr and Al occurs on the surface of Cr_2AlC powder in air (Ref 40). After deconvolution, Cr2*p* spectra revealed four peaks i.e., Cr-C bond peaks at binding energy 573.5 and 583.4 eV. Similar observations were made by Shtansky et al. and Zhang et al.(Ref 41, 42) and Cr-O bond peaks at binding energy 576.18 and 586.9 eV corresponding to Cr_2O_3 which is in sync with observations by Sleight and Agostinelli (Ref 43, 44). Similarly, after deconvolution the Al 2p spectra revealed two peaks: Al-O bond peaks at binding energies of 71.25 and 74.3 eV corresponding to Al_2O_3, the similar peak positions were observed by Gillet et al. and Ertl et al. (Ref 45, 46). The aluminum (Al) component within Cr_2AlC forms a bond characterized by a weak electrostatic force, rendering it susceptible to oxidation. This tendency of Al to oxidize is in alignment with the findings presented by Naslund et al. and Desai et al., who have noted the weak electrostatic nature of Al bonds in MAX phases containing aluminum (Ref 47, 48). Furthermore, the work of Baben et al. highlights instances of oxygen incorporation in M_2AlC. (Ref 49). After deconvolution, the C1s spectra showed four peaks located at 282.1, 284.6, 285.9 and 288.6 eV, respectively. The peak observed at 282.1 can be attributed to the typical carbon valence state for carbon that is carbide-like i.e., Cr-C as reported by Shtansky et al. (Ref 41). The peaks located at 284.6 and 285.94 eV corresponds to basic C-C bond. Identical observations were observed by Abdelkader et al. and Moncoffre et al. (Ref 40, 50). Additionally, the presence of C-O bond is detected at the peak located at 288.6 eV in line with the observation of Moncoffre, N et al. (Ref 50). Although oxygen is not inherently present in Cr_2AlC; the samples were exposed to laboratory atmosphere condition and hence, the possibility of O being present in the form of Cr_2O_3 as well as Al_2O_3 needs to be further investigated. The O1s spectra were deconvoluted, revealing two peaks at 529.9 and 531.7 eV, corresponding to the Cr-O bond of Cr_2O_3 and the Al-O bond of Al_2O_3, Stypula, B, and Stypula, B et al. have reported comparable binding energies associated with Cr_2O_3 and Al_2O_3 (Ref 51, 52).

3.6 High Temperature XRD

High Temperature x-ray diffraction studies were performed for investigating the thermal stability of synthesized Cr_2AlC. If the Al is weakly bonded in the MAX phase material, it could get oxidized as the temperature increases. Further, it could also get evaporated at the prevailing temperatures of the high temperature XRD test, as this test is conducted at sub-atmospheric pressures, viz. around 5×10^{-2} mbar. The results of this high temperature XRD tests – performed at various temperatures ranging from room temperature to 1000 °C – are shown in Fig. 8. From the results, it is observed that the peak positions of Cr_2AlC slightly shifted with at higher temperatures. Possible reason for this finding may be because of thermal expansion. Further it is also observed that the intensities of Cr_2AlC peaks decreased with increasing temperatures. However, there is no indication on the formation of Al_2O_3 or any other oxide or any other impurity, with the increase in temperature up to 1000 °C. These results confirm about the phase stability of the synthesized Cr_2AlC up to 1000 °C, in the sub-atmospheric low pressure conditions.

3.7 TG-DSC

The synthesized Cr_2AlC was subjected to TG-DSC studies also, in order to analyze its thermal stability. The tests were performed at sub-atmospheric pressure conditions, viz. at around 5×10^{-2} mbar and the temperature was increased up to 1400 °C. The results of TG-DSC studies are shown in Fig. 9.

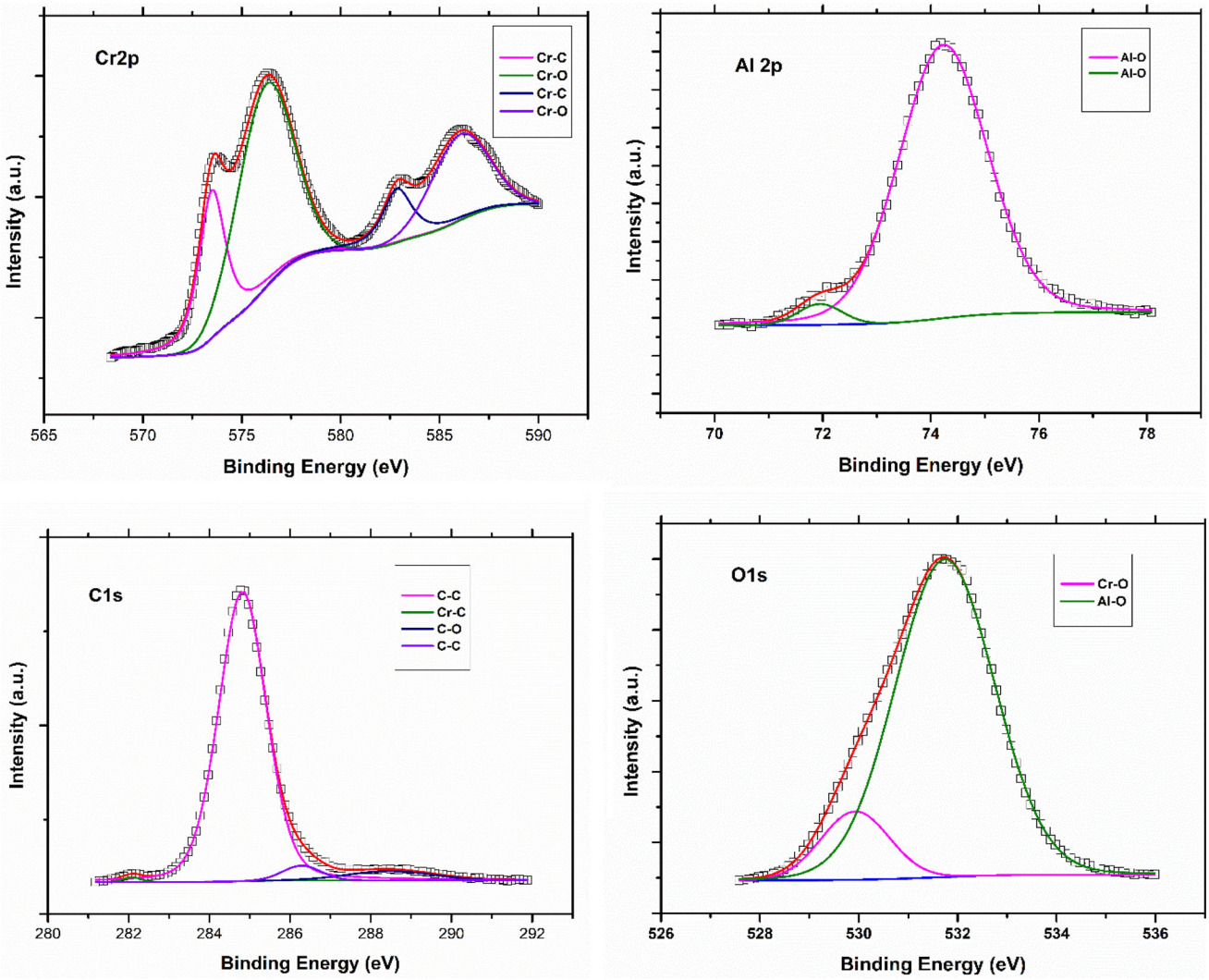

Fig. 7 XPS high-resolution spectra of the as synthesized Cr_2AlC MAX phase

The TG curve indicates that the rate of oxidation increases in direct correlation to the temperature of the test. Further, it has also revealed that there is an approximate 2% weight gain in the sample after TG test, possibility of surface oxidation of the sample. On the other hand, the DSC curve reveals that below 785 °C the primary reaction was endothermic, attributed to sample heating. However, above 785 °C the dominant reaction became exothermic, indicating the oxidation of Cr_2AlC. It is the inherent property of Cr_2AlC to form a continuous protective surface layer of Al_2O_3 when subjected to high temperature (Ref 8). Consequently, noticeable oxidation of Cr_2AlC commences above 785 °C (Ref 53). Whenever Cr_2AlC underwent oxidation, it produces a layer of Al_2O_3 on the surface. In addition, the consumption of Al during this process causes the formation of a layer of Cr_7C_3 underneath the Al_2O_3 layer. This layer of Cr_7C_3 is known for its hardness and is stabilized by strong interactions between Cr and C atoms (Ref 53).

Samples, after TG-DSC studies, were subjected again to XRD analysis in order to investigate the new phases that might have formed during TG test which must have contributed to increase in weight. They were also analyzed with SEM to check for any morphological changes occurred during TG-DSC test. The x-ray diffraction (XRD) results are shown in Fig. 10. The primary peaks are identified with Cr_2AlC phase, while additional peaks representing Al_2O_3 (ICDD 00-001-1296) and Cr_7C3 (03-065-1347) were also detected. SEM results also complemented these findings. SEM micrographs, shown in Fig. 11, clearly indicate the appearance of flower-like morphology, which is associated with α-Al_2O_3 (Ref 50); along with regular Cr_2AlC. SEM energy-dispersive spectroscopy (EDS) analysis was conducted at a few points, and the results are shown in Table 3. EDS results of P4, P5 and P6 data points substantiate the coexistence of Al_2O_3 and Cr_2AlC. This particular oxidation of aluminum primarily occurred on the surface, potentially resulting in the transformation of Cr_2AlC into Cr_3C_7 and Al_2O_3 in the top layers. The oxidation of aluminum in Cr_2AlC can be attributed to two factors: its higher affinity for oxygen when compared to chromium and carbon, and the greater Gibbs free energy for the reaction between aluminum and oxygen compared to other elements such as chromium and carbon.

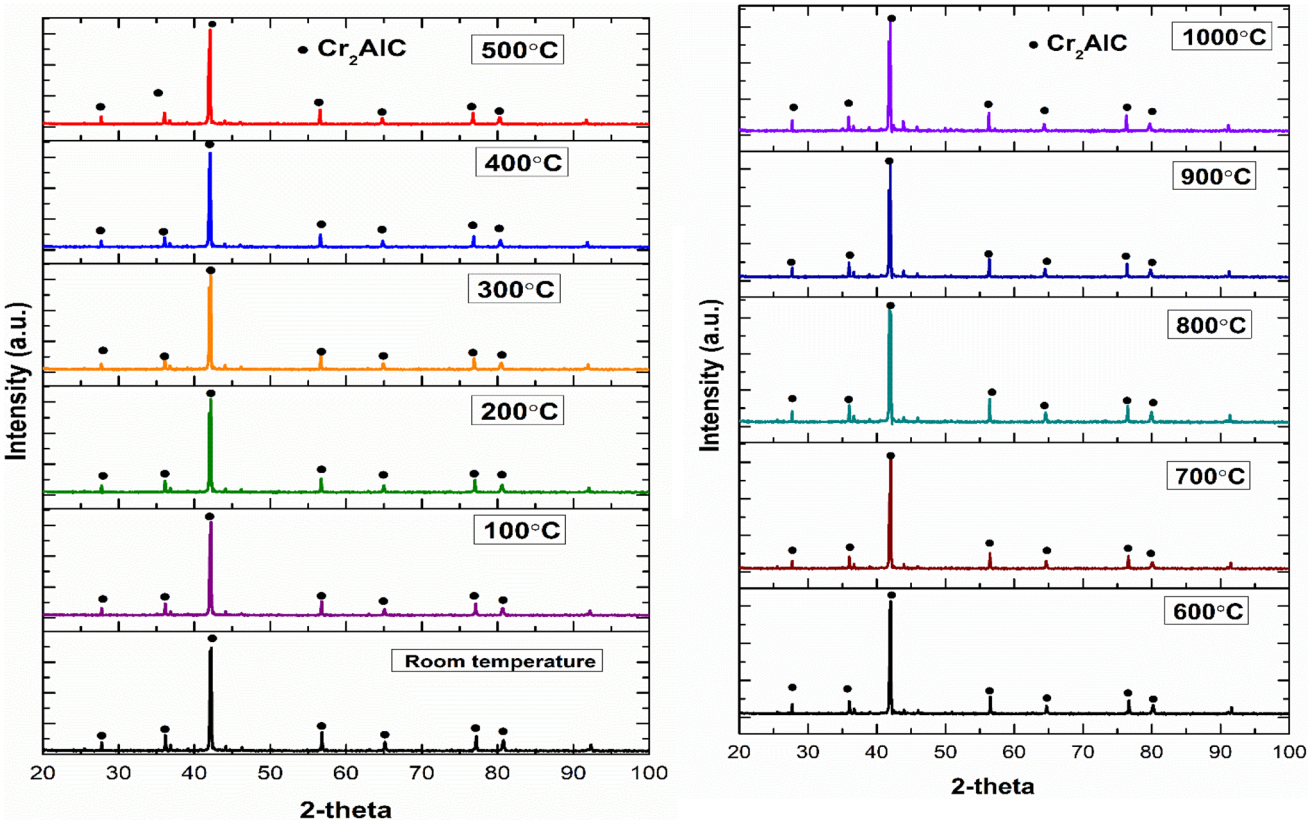

Fig. 8 HT-XRD graphs of as synthesized Cr_2AlC Powder

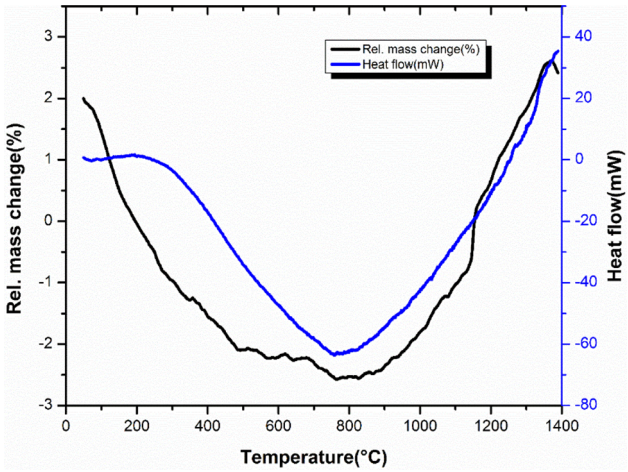

Fig. 9 TG-DSC curve of as synthesized Cr_2AlC MAX phase powder

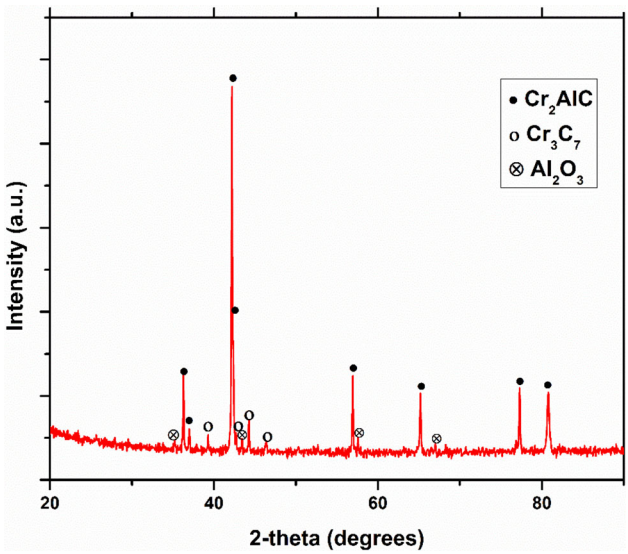

Fig. 10 XRD pattern of Cr_2AlC DSC sample

4. Conclusions

A new two-step pressureless sintering process was successfully employed for producing high purity Cr_2AlC powders using commercially available Cr, Al, and C powders. Liquid-solid reactions between Al and Cr, respectively, in the first step were used for the formation of Chromium Aluminide intermetallics. A full reaction between these intermetallics and Carbon is ensured in the second step (at 1350 °C). Formation of pure Cr_2AlC is confirmed through x-ray Diffraction and Raman spectroscopy analyses. Scanning electron microscopy (SEM) results provided evidence on the existence of layered morphology of Cr_2AlC grains; while the EPMA quantitative elemental analysis resulted in atomic percentages of 52.99% Cr, 22.81% Al, and 24.19% C and are found to be aligning with XRD findings.

Additional insights from x-ray Photoelectron Spectroscopy (XPS) investigations unveiled the bonding nature, with Cr-C bonding being identified. HT-XRD studies, conducted at various temperatures, confirmed that there is no oxide forma-

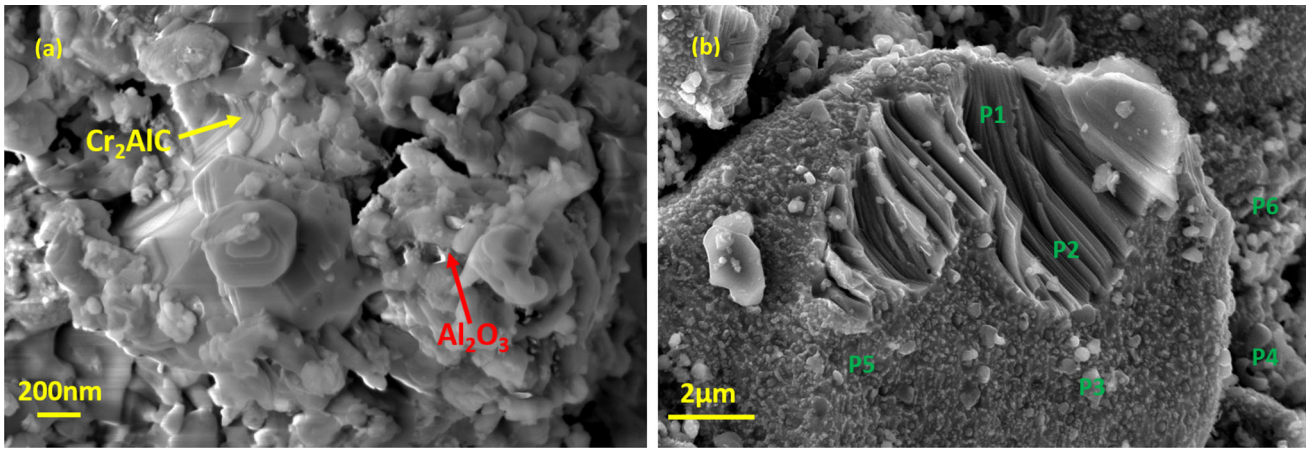

Fig. 11 (a) SEM image of DSC Cr_2AlC sample (b) EDS spot point locations

Table 3 Atomic percentage of Cr, Al, C and O in DSC Cr_2AlC powder sample

Spectrum	Cr	Al	C	O
P1	51.32	22.45	25.2	1.03
P2	50.67	19.96	29.37	…
P3	51.90	21.09	24.41	2.60
P4	50.96	5.44	33.84	9.76
P5	31.97	9.35	31.7	17.95
P6	25.13	10.55	50.83	15.93

tion up to 1000 °C indicating of the Cr_2AlC phase stability. However, Differential scanning calorimetry (DSC) data demonstrated the onset of oxide formation after 785 °C, and thermogravimetric analysis (TG) revealed an approximate 2% increase in weight, corroborating the occurrence of oxidation. XRD and SEM (EDS) analysis of post TG-DSC samples confirmed the presence of Al_2O_3. This is leading us to conclude that there is oxide formation with increase in temperature but only through a few layers on the surface and is not in considerable quantity to be identified in HT-XRD up to 1000 °C. Oxidation is relatively higher during TG-DSC tests as they were conducted up to 1400 °C, and the same was reflected through increase in weight by approximately 2% and presence of oxide peaks in XRD results of post TG-DSC samples.

These comprehensive analyses collectively affirm the successful synthesis of Cr_2AlC powders with high purity and reveal valuable insights into the fundamental properties of the material.

Funding

Open access funding provided by Department of Atomic Energy.

Data Availability

The raw/processed data required to reproduce these findings cannot be shared at this time as the data also form part of an ongoing study.

Consent for Publication

During the preparation of this work the author(s) used Quill bot] in order to improve the readability and grammar. After using this tool/service, the author(s) reviewed and edited the content as needed and take(s) full responsibility for the content of the publication.

Open Access

References

1. M.W. Barsoum, The MN+ 1AXN Phases: A New Class of Solids: Thermodynamically Stable Nanolaminates, *Prog. Solid State Chem.*, 2000, **28**(1–4), p 201–281
2. M.W. Barsoum and M. Radovic, Elastic and Mechanical Properties of the MAX Phases, *Annu. Rev. Mater. Res.*, 2011, **41**, p 195–227
3. X. He et al., General Trends in the Structural, Electronic and elastic Properties of the M3AlC2 Phases (M= transition metal): A First-Principle Study, *Comput. Mater. Sci.*, 2010, **49**(3), p 691–698
4. M.W. Barsoum, D. Brodkin, and T. El-Raghy, Layered Machinable Ceramics for High Temperature Applications, *Scripta Mater.*, 1997, **36**(5), p 535–541
5. T. Scabarozi et al., Thermal Expansion of Select $M_{n+1}AX_n$ (M = Early Transition Metal, A = A Group Element, X = C or N) Phases Measured by High Temperature X-ray Diffraction and Dilatometry, *J. Appl. Phys.*, 2009, **105**(1), 013543
6. M. Radovic and M.W. Barsoum, MAX Phases: Bridging the Gap Between Metals and Ceramics, *Am. Ceram. Soc. Bull.*, 2013, **92**(3), p 20–27

7. Z. Lin et al., High-Temperature Oxidation and Hot Corrosion of Cr_2AlC, *Acta Mater.*, 2007, **55**(18), p 6182–6191
8. J. Gonzalez-Julian, Processing of MAX Phases: From Synthesis to Applications, *J. Am. Ceram. Soc.*, 2021, **104**(2), p 659–690
9. W. Jeitschko, H. Nowotny, and F. Benesovsky, Kohlenstoffhaltige ternäre Verbindungen (H-phase), *Monatshef. Chem. Verwandte Teile anderer Wissenschaften*, 1963, **94**(4), p 672–676
10. J. Schuster, H. Nowotny, and C. Vaccaro, The Ternary Systems: CrAlC, VAlC, and TiAlC and the Behavior of H-Phases (M2AlC), *J. Solid State Chem.*, 1980, **32**(2), p 213–219
11. M. Imtyazuddin, A.H. Mir, M.A. Tunes, and V.M. Vishnyakov, Radiation Resistance and Mechanical Properties of Magnetron-Sputtered Cr2AlC Thin Films, *J. Nucl. Mater.*, 2019, **526**, p 151742. https://doi.org/10.1016/j.jnucmat.2019.151742
12. W. Tian et al., Mechanical Properties of Pulse Discharge Sintered Cr2AlC at 25–1000° C, *Mater. Lett.*, 2009, **63**(8), p 670–672
13. W. Tian et al., Synthesis and Thermal and Electrical Properties of Bulk Cr_2AlC, *Scripta Mater.*, 2006, **54**(5), p 841–846
14. D. Lee and T.D. Nguyen, Cyclic Oxidation of Cr_2AlC Between 1000 and 1300° C in Air, *J. Alloys Compd.*, 2008, **464**(1–2), p 434–439
15. B.S. Reghunath, D. Davis, and K.S. Devi, Synthesis and Characterization of Cr2AlC MAX Phase for Photocatalytic Applications, *Chemosphere*, 2021, **283**, 131281
16. L.-O. Xiao et al., Synthesis and Thermal Stability of Cr_2AlC, *J. Eur. Ceram. Soc.*, 2011, **31**(8), p 1497–1502
17. S. Li et al., Mechanical Properties of Low Temperature Synthesized Dense and Fine-grained Cr_2AlC Ceramics, *J. Eur. Ceram. Soc.*, 2011, **31**(1–2), p 217–224
18. W. Tian et al., Synthesis Reactions of Cr_2AlC from Cr-Al_4C_3-C by Pulse Discharge Sintering, *Mater. Lett.*, 2008, **62**(23), p 3852–3855
19. W.-B. Tian, P.-L. Wang, Y.-M. Kan, and G.-Jn. Zhang, Cr_2AlC Powders Prepared by Molten Salt Method, *J. Alloys Compd.*, 2008, **461**(1–2), p L5–L10. https://doi.org/10.1016/j.jallcom.2007.06.094
20. B. Manoun et al., Compression Behavior of M_2Al C (M= Ti, V, Cr, Nb, and Ta) Phases to Above 50 GPa, *Phys. Rev. B*, 2006, **73**(2), 024110
21. V. Gorshkov et al., SHS Metallurgy of Cr_2AlC MAX Phase-Based Cast Materials, *Russ. J. Non-Ferrous Met.*, 2018, **59**(5), p 570–575
22. M. Yan et al., Effect of Ball Milling Treatment on the Microstructures and Properties of Cr_2AlC Powders and Hot Pressed Bulk Ceramics, *J. Eur. Ceram. Soc.*, 2019, **39**(16), p 5140–5148
23. Z. Lin et al., In-situ Hot Pressing/Solid-Liquid Reaction Synthesis of Bulk Cr_2AlC, *Int. J. Mater. Res.*, 2005, **96**(3), p 291–296
24. H.-C. Oh, S.-H. Lee, and S.-C. Choi, The Reaction Mechanism for the Low Temperature Synthesis of Cr_2AlC under Electronic Field, *J. Alloys Compd.*, 2014, **587**, p 296–302
25. W.-B. Tian et al., Phase Formation Sequence of Cr_2AlC Ceramics Starting from Cr-Al-C Powders, *Mater. Sci. Eng.A*, 2007, **443**(1–2), p 229–234
26. G. Ying et al., Synthesis and Mechanical Properties of High-Purity Cr_2AlC Ceramic, *Mater. Sci. Eng.*, 2011, **528**(6), p 2635–2640
27. J. Gonzalez-Julian et al., Effect of Sintering Method on the Microstructure of Pure Cr_2AlC MAX Phase Ceramics, *J. Ceram. Soc. Jpn.*, 2016, **124**(4), p 415–420
28. B.B. Panigrahi et al., Reaction Synthesis and Pressureless Sintering of Cr_2AlC Powder, *J. Am. Ceram. Soc.*, 2010, **93**(6), p 1530–1533
29. I.M. Low, Z. Oo, and K. Prince, Effect of Vacuum Annealing on the Phase Stability of Ti_3SiC_2, *J. Am. Ceram. Soc.*, 2007, **90**(8), p 2610–2614
30. C. Racault, F. Langlais, and R. Naslain, Solid-State Synthesis and Characterization of the Ternary Phase Ti_3SiC_2, *J. Mater. Sci.*, 1994, **29**(13), p 3384–3392
31. Z. Oo, I. Low, and B. O'Connor, Dynamic Study of the Thermal Stability of Impure Ti_3SiC_2 in Argon and Air by Neutron Diffraction, *Phys. B*, 2006, **385**, p 499–501
32. S.-B. Li et al., Synthesis and Microstructure of Ti_3AlC_2 by Mechanically Activated Sintering of Elemental Powders, *Ceram. Int.*, 2007, **33**(2), p 169–173
33. W.K. Pang, I.M. Low, and Z.M. Sun, In situ High-Temperature Diffraction Study of the Thermal Dissociation of Ti_3AlC_2 in Vacuum, *J. Am. Ceram. Soc.*, 2010, **93**(9), p 2871–2876
34. D. Lee and S. Park, Oxidation of Cr2AlC Between 900 and 1200 °C in Air, *Oxid. Met.*, 2007, **68**(5), p 211–222
35. K. Hall et al., Synthesis and Characterization of Novel Polymer Matrix Composites Reinforced with Max Phases (Ti_3SiC_2, Ti_3AlC_2, and Cr_2AlC) or MoAlB by Fused Deposition Modeling, *Int. J. Ceram. Eng.*, 2019, **1**(3), p 144–154
36. K.Y. Karuna et al., Nanocrystalline Cr2AlC-MAX Phase Formation During Mechanically Activated Annealing of Al-31Cr-7C, *Trans. Indian Inst. Met*, 2021, **74**(9), p 2313–2318. https://doi.org/10.1007/s12666-021-02324-4
37. J.E. Spanier et al., Vibrational Behavior of the $M_{n+1}AX_n$ Phases from First-order Raman Scattering (M = Ti, V, Cr, A = Si, X = C, N), *Phys. Rev. B*, 2005, **71**(1), 012103
38. O.D. Leaffer et al., On Raman Scattering from Selected M2AC Compounds, *J. Mater. Res.*, 2007, **22**(10), p 2651–2654
39. J. Wang et al., Raman Active Phonon Modes and Heat Capacities of Ti_2AlC and Cr_2AlC Ceramics: First-Principles and Experimental Investigations, *Appl. Phys. Lett.*, 2005, **86**(10), 101902
40. A.M.J. Abdelkader, Molten Salts Electrochemical Synthesis of Cr_2AlC, *J. Eur. Ceram. Soc.*, 2016, **36**(1), p 33–42
41. D. Shtansky et al., Comparative Investigation of TiAlC (N), TiCrAlC (N), and CrAlC (N) Coatings Deposited by Sputtering of MAX-Phase $Ti_{2-x}Cr_xAlC$ Targets, *Surf. Coat. Technol.*, 2009, **203**(23), p 3595–3609
42. Y. Zhang et al., High Antioxidant Lamellar Structure Cr_2AlC: Dielectric and Microwave Absorption Properties in X Band, *J. Alloys Compd.*, 2021, **860**, 157896
43. C. Sleigh et al., On the Determination of Atomic Charge Via ESCA Including Application to Organometallics, *J. Electron Spectrosc. Relat. phenom.*, 1996, **77**(1), p 41–57
44. E. Agostinelli et al., An XPS Study of the Electronic Structure of the $Zn_xCd_{1-x}Cr_2$ (X = S, Se) Spinel System, *J. Phys.*, 1989, **50**(3), p 269–272
45. E. Gillet and B. Ealet, Characterization of Sapphire Surfaces by Electron Energy-Loss Spectroscopy, *Surf. Sci.*, 1992, **273**(3), p 427–436
46. G. Ertl et al., XPS Study of Copper Aluminate Catalysts, *Appl. Surf. Sci.*, 1980, **5**(1), p 49–64
47. V. Desai et al., Pressureless Manufacturing of High Purity Ti_3AlC_2 MAX Phase Material: Synthesis and Characterisation, *Vacuum*, 2023, **214**, p 112221. https://doi.org/10.1016/j.vacuum.2023.112221
48. L.-Å. Näslund, P.O.Å. Persson, and J. Rosen, X-ray Photoelectron Spectroscopy of Ti_3AlC_2, Ti_3C2Tz, and TiC Provides Evidence for the Electrostatic Interaction between Laminated Layers in MAX-Phase Materials, *J. Phys. Chem. C*, 2020, **124**(50), p 27732–27742. https://doi.org/10.1021/acs.jpcc.0c07413
49. M. Baben et al., Oxygen Incorporation in M_2AlC (M = Ti, V, Cr), *Acta Mater.*, 2012, **60**(12), p 4810–4818
50. N. Moncoffre et al., Temperature Influence During Nitrogen Implantation Into Steel, *Nuclear Instrum. Methods Phys. Rese. Sect. B Beam Interact. Mater. Atoms*, 1985, **7**, p 177–183
51. B. Stypula and J. Stoch, The Characterization of Passive Films on Chromium Electrodes by XPS, *Corros. Sci.*, 1994, **36**(12), p 2159–2167
52. B.R. Strohmeier, Characterization of an Activated Alumina Claus Catalyst by XPS, *Surf. Sci. Spectra*, 1994, **3**(2), p 141–146
53. D.B. Lee and S.W. Park, Oxidation of Cr_2AlC Between 900 and 1200 °C in Air, *Oxidat. Met.*, 2007, **68**(5–6), p 211–222. https://doi.org/10.1007/s11085-007-9071-0